Journal of
Marine Science and Engineering

MDPI

Article

On the Influence of Beach Slope on Wave Non-Linearities on a Macrotidal Low-Tide Terrace Beach

Amadou Diouf [1,2], France Floc'h [2,*], Bamol Ali Sow [1], Charles Caulet [3] and Emmanuel Augereau [2]

[1] Laboratoire d'Océanographie, des Sciences de l'Environnement et du Climat (LOSEC), Université Assane Seck, Ziguinchor BP 523, Senegal; dioufamadou75@gmail.com (A.D.); bsow@univ-zig.sn (B.A.S.)
[2] Univ Brest, CNRS, Geo-Ocean UMR6538, F-29280 Plouzané, France; emmanuel.augereau@univ-brest.fr
[3] Geography Department, Research Chair in Coastal Geoscience, Université du Québec à Rimouski, 300 Allée des Ursulines, Rimouski, QC G5L 3A1, Canada; charles_caulet@uqar.ca
* Correspondence: france.floch@univ-brest.fr

Abstract: This study examines the evolution of wave shapes as they propagate over a beach of varying morphology, information essential for understanding coastal dynamics and supporting coastal management. Our objective was to analyze the relationship between wave shape parameters and the local slope of the beach. To achieve this, we used data from pressure sensors and topographic measurements to evaluate the shape of waves on a cross-shore profile of a low-tide terrace beach. The analysis of wave conditions revealed a pronounced modulation of the tidal signal, which is augmented during storm events. Our findings demonstrate that the asymmetry and skewness parameters are more pronounced in the reflective zone of the beach. Considering these results, it can be concluded that the non-linearity of waves is significantly affected by the beach slope. The parameterization method employed in this study effectively incorporates this factor, offering improved accuracy in comparison to the existing approaches.

Keywords: wave shape; non-linearities; beach slope; macrotidal

Citation: Diouf, A.; Floc'h, F.; Sow, B.A.; Caulet, C.; Augereau, E. On the Influence of Beach Slope on Wave Non-Linearities on a Macrotidal Low-Tide Terrace Beach. *J. Mar. Sci. Eng.* **2024**, *12*, 1997. https://doi.org/10.3390/jmse12111997

Academic Editor: Lev Shemer

Received: 24 September 2024
Revised: 15 October 2024
Accepted: 17 October 2024
Published: 6 November 2024

1. Introduction

Approximately 10% of the world's population live in coastal areas that are less than 10 m above mean sea level [1]. These regions are experiencing increasing population density due to the high rates of population growth and urbanization [2]. At the same time, the analysis of satellite-derived shoreline data reveals that 24% of the world's sandy beaches are eroding faster than 0.5 m/year, while 28% are accreting and 48% are stable [3]. In Europe, coastal erosion affects 20% of the coastline, resulting in an annual loss of 15 km^2 [4]. Coastal areas are also susceptible to marine hazards such as flooding and erosion. Sandy coasts, which are highly dynamic and can change in response to extreme marine events, are one of the most vulnerable types of coasts [2]. Numerous studies have shown the impact of open sea swell climate on beach morphology with regard to the risks of disasters linked to interactions between waves and morphology [5,6]. The energy released when waves break is transformed into potential energy (water level above the coast) and kinetic energy (the generation of coastal currents). In shallow waters, wave frequencies undergo non-linear interactions, leading to an increase in high frequencies and the deformation of the free surface. This causes the waves to straighten and then break. Furthermore, wave non-linearities have been shown to be among the main drivers of sediment transport [7,8], becoming non-negligible during wave shoaling and breaking processes. This results in wave asymmetry and skewness, inducing shear stress asymmetry and skewness in the wave boundary layer [9–12] that leads to strong net sand transport directed on-shore or off-shore depending on the incident conditions [7,13,14]. The bed slope has also been found to influence interactions between waves, enhancing non-linearities close to the breaking point [15] or causing strong wave reflection on the beach, reducing the wave velocity

skewness [14]. More recently, the wind direction has been shown to have a major influence on the maximum non-linearity reached by waves during their propagation to the coast in a sheltered environment [16].

Several parameterizations of wave asymmetry and skewness have been proposed based on the Ursell number, according to either 1/observational data [17–20] or 2/numerical data from the wave-resolved model, including the beach slope influence [21]. However, data scatter around the fitted formulae remains broad. The scientific issues raised in the literature center on the lack of in situ observations of wave shape in the surf zone across a broad diversity. Such observations would improve our understanding of the wave transformation process, which constrains sediment transport and thus beach morphodynamics, particularly during accretive periods.

A measurement campaign was conducted from 3 October to 3 November 2016 at Porsmilin, located in Anse de Bertheaume (France). Porsmilin is one of the sites of the DYNALIT National Observation Service, surveyed monthly for the last twenty years. The purpose of this campaign was to gain a better understanding of wave transformation across a cross-shore 'low tide terrace' beach profile using 17 wave gauges positioned all over the foreshore of this macrotidal beach (over 200 m) plus another off-shore at a depth of 15 m, as well as the daily surveys of the beach profile. The data obtained during this campaign provide valuable insights into this wave shape transformation in the near-shore.

2. Methods

2.1. Wave Gauges Processing

Pressure transducers were used to acquire 10 Hz pressure data. Their position was recorded by Differential Global Positioning System (DGPS) every day to ensure there was no day-to-day displacement. The pressure data were corrected from atmospheric mean sea level pressure recorded at the Brest-Guipavas Meteo France station. Only the gravity part of the pressure signal was considered (incident gravity band from 0.04 Hz to 0.4 Hz). The pressure at the bottom is considered to avoid uncertainties due to linear or non-linear sea surface reconstruction [16]. The surface elevation η is thus reconstructed via hydrostatic formulation. To estimate velocity u_η from bottom pressure measurements (Equation (1)), the linear theory was considered at intermediate water depths, including a dependence on water depth [21]):

$$u_\eta = \sum_i \eta_i \omega_i \frac{\cosh k_i(z_0 + h)}{\sinh(k_i h)} \quad (1)$$

where the index i represents each of the frequencies that transferred from the free-surface elevation time series to the velocity time series, k_i is the wave number, z_0 is the depth at which u_η is calculated, and h is the local water depth. k_i is obtained from the dispersion relation, which can be expressed, for each frequency, as

$$\omega_i^2 = g k_i \tanh(k_i h) \quad (2)$$

where g is the gravitational acceleration and ω_i is the angular frequency.

To retrieve the wave spectrum and wave-averaged parameters, the Fourier transforms of the detrended water level were used. The Fast Fourier Transform (FFT) method was applied over 2048 data points for the incident gravity wave band. Since the signal was not perfectly periodic, a leakage issue could induce artifacts in the resulting spectrum. To avoid this, a Hamming window was applied to the signal, leading to zero values at the edges. An average was made over several contiguous spectra with 50% overlap. For the incident band, an average was made over 20 min [22]. The mean spectral wave parameters, i.e., the significant wave height H_{m0} and the equivalent spectral mean period $T_{m0;-1}$, were then computed.

2.2. Wave Non-Linearities

The evolution of wave non-linearities along the cross-shore profile of the beach reflects the changes in waveform as they propagate towards the surf zone. Asymmetrical waves are characterized by a high, narrow crest and a wider but shallow trough, creating a forward-leaning sawtooth shape. Several authors have attempted to explain wave non-linearity based on asymmetry (As) [8,16–21].

$$\mathrm{As}_\eta = \frac{-\langle \mathcal{H}(\eta - \overline{\eta})^3 \rangle}{\sigma^3} \tag{3}$$

where $\mathcal{H}$ is the imaginary part of the Hilbert transform of the free surface residual $(\eta - \overline{\eta})$, where η denotes the mean surface elevation and σ its standard deviation. <.> represents the arithmetic average operation.

The interaction of the triads results in non-linear energy transfers, causing waves to experience an increase in crest height and a flattening of troughs as they move towards shallower water [23–25]. Hence, there is an increase in wave skewness:

$$\mathrm{Sk}_\eta = \frac{\langle (\eta - \overline{\eta})^3 \rangle}{\sigma^3} \tag{4}$$

In addition to these two parameters, we also calculated asymmetry As_u and skewness Sk_u replacing η by u in Equations (3) and (4). It leads to B, the combined non-linear parameter for wave orbital velocity:

$$\mathrm{B} = \sqrt{\mathrm{As}_u^2 + \mathrm{Sk}_u^2} \tag{5}$$

Many empirical studies have tried to predict these parameters to characterize wave behavior based on local parameters and beach morphodynamic conditions. The Ursell number, denoted by Ur, is a dimensionless parameter used to characterize the significance of non-linear effects on surface waves, especially as they propagate into shallow waters where these effects can strongly influence wave behavior and breaking [17]. It is defined in terms of the significant wave height (H_{m0}), the water depth (h), and the wave number (k). The Ursell number is formally defined as follows:

$$\mathrm{Ur} = \frac{3\mathrm{H}_{m0}\mathrm{k}}{8(\mathrm{kh})^3} \tag{6}$$

The local wave number, k, is calculated using the linear theory with the mean period $\mathrm{Tm} = \frac{m_0}{m_1}$, where m_n is the spectral moment of order n. The local depth can be recovered from each sensor, while H_{m0} represents the local significant wave height.

Parameter B is employed to delineate the evolution of orbital velocity asymmetries of waves as they propagate towards the shore and break. It is a valuable tool for elucidating the fundamental processes underlying the transformation of wave characteristics, with particular emphasis on orbital velocity asymmetries (Equation (5)). Refs. [17,18] proposed parameterizations based on the Ursell number to estimate the total non-linearity parameter B (B_{DB95} Equation (7) and B_{R12} Equation (8), respectively).

$$\mathrm{B}_{\mathrm{DB95}} = 0.8 + 0.62\log(\mathrm{Ur}) \tag{7}$$

$$\mathrm{B}_{\mathrm{R12}} = \mathrm{p}_1 + \frac{\mathrm{p}_2 - \mathrm{p}_1}{1 + \exp\frac{\mathrm{p}_3 - \log \mathrm{Ur}}{\mathrm{p}_4}} \tag{8}$$

where p_1 and p_2 represent the limits of B as Ur tends to 0 and infinity, respectively; p_3 is related to the inflection point; and p_4 measures the slope. Using $p_1 = 0$ and a non-linear least squares fit, Ref. [18] found $p_2 = 0.857 \pm 0.016$; $p_3 = -0.471 \pm 0.025$ and $p_4 = 0.297 \pm 0.021$, where $\pm$ represents the 95% confidence interval.

For the subsequent phase of this research, we used a logarithmic scale will be employed to ascertain the observed correlation between the asymmetry, skewness of gravity waves, and the Ursell number calculated from pressure transducers.

2.3. The Role of Slope

Slope plays an essential role in characterizing beach morphodynamics. Slope variability may cause changes in asymmetry, stretching, sediment transport processes, and morphology [25]. Previous studies have demonstrated the significance of slope in nonlinear wave interactions [8]. Some beaches may display highly contrasting dynamics due to slope heterogeneity. These include intermediate-type beaches like the one at Porsmilin, which is reflective at the top and dissipative at the bottom. It is evident that the slope can affect the shape of waves that propagate along the cross-shore profile of the beach.

Ref. [8] included a parameter called NP0 including the influence of the beach slope, and the breaking index γ in [18] the formula (Equation (8)) in the term p2 according to numerical results, as $p_2 = B_{max} = q_1 NP0^{q_2} + q_3\gamma^{q_4} + q_5$ with q_1 = 0.16 +/− 0.06, q_2 = −0.19 +/− 0.04, q_3 = −0.33 +/− 0.12, q_4 = −0.22 +/− 0.18, and q_5 = 0.19 +/− 0.13, where the range represented by the ± values is the 95% confidence interval. The parameter NP0 (Equation (9)) considers the influence of the local beach slope through the Iribarren number (Ib), with $\mathrm{Ib} = \tan\beta / \sqrt{\left(\frac{H_0}{L_0}\right)}$, and the steepness of the waves off-shore the coast through the ratio $\left(\frac{H_0}{L_0}\right)^2$ using off-shore wave height H_0 and off-shore wavelength L_0:

$$\mathrm{NP0} = \mathrm{Ib}\left(\frac{H_0}{L_0}\right)^2 \tag{9}$$

2.4. Study Site

The data were obtained during the DYNATREZII measurement campaign at Porsmilin Beach, France (Figure 1) [26]. According to the classification by [5], based on dimensionless fall velocity and a tide-dominated environment (RTR > 7), this beach belongs to the category of intermediate beaches. These beaches exhibit a discontinuity that is manifested by a distinct division of their profile into two parts: an upper part with a steeper and more reflective slope ($\beta \sim 0.08$), and a lower part that is gentler and of a dissipative nature ($\beta \sim 0.01$–0.02). These are called low-tide terraces (LTTs) because the lower part of the beach, which is exposed during low tides, forms a dissipative terrace (Figure 1c). An LTT typically has coarse sand with gravel or even pebbles on the reflective part of its profile, while the lower part of the beach is made up of fine and cohesive sediments. On Porsmilin Beach, the sediment size remains quite homogeneous (D_{50} = 320 µm) with the appearance of pebbles in the intermediate part of the beach (between the reflective and dissipative parts) during energetic events [26–29].

The DYNATREZII campaign was carried out between 14 October and 3 November 2016 using 15 co-located pressure transducers positioned in a cross-shore network (+2 in longshore to address longshore variability, see PT 16 and 17 on Figure 1b). The deepest sensor on the beach is approximately 5 m deep at high tide, at the bottom of the intertidal zone. These pressure transducers had an acquisition frequency of 10 Hz and were immersed in the ground to a depth of around 15 cm. The topographic surveys of the beach following the cross-shore profiles (Figure 1a,b) were carried out from the top of the beach to the shoreline [27] over about 20 days, showing no significant transport during the experiment (local bed slope variation does not exceed 5%). Additionally, a 16-beams Velodyne© LiDAR profiler collected free-surface fluctuations on the upper beach, between the inner surf zone and the swash zone from 40 to 80 m of the beach profile (Figure 1d), at high tide on the 17th, 19th, 21st, 24th, 26th, and 28th of October.

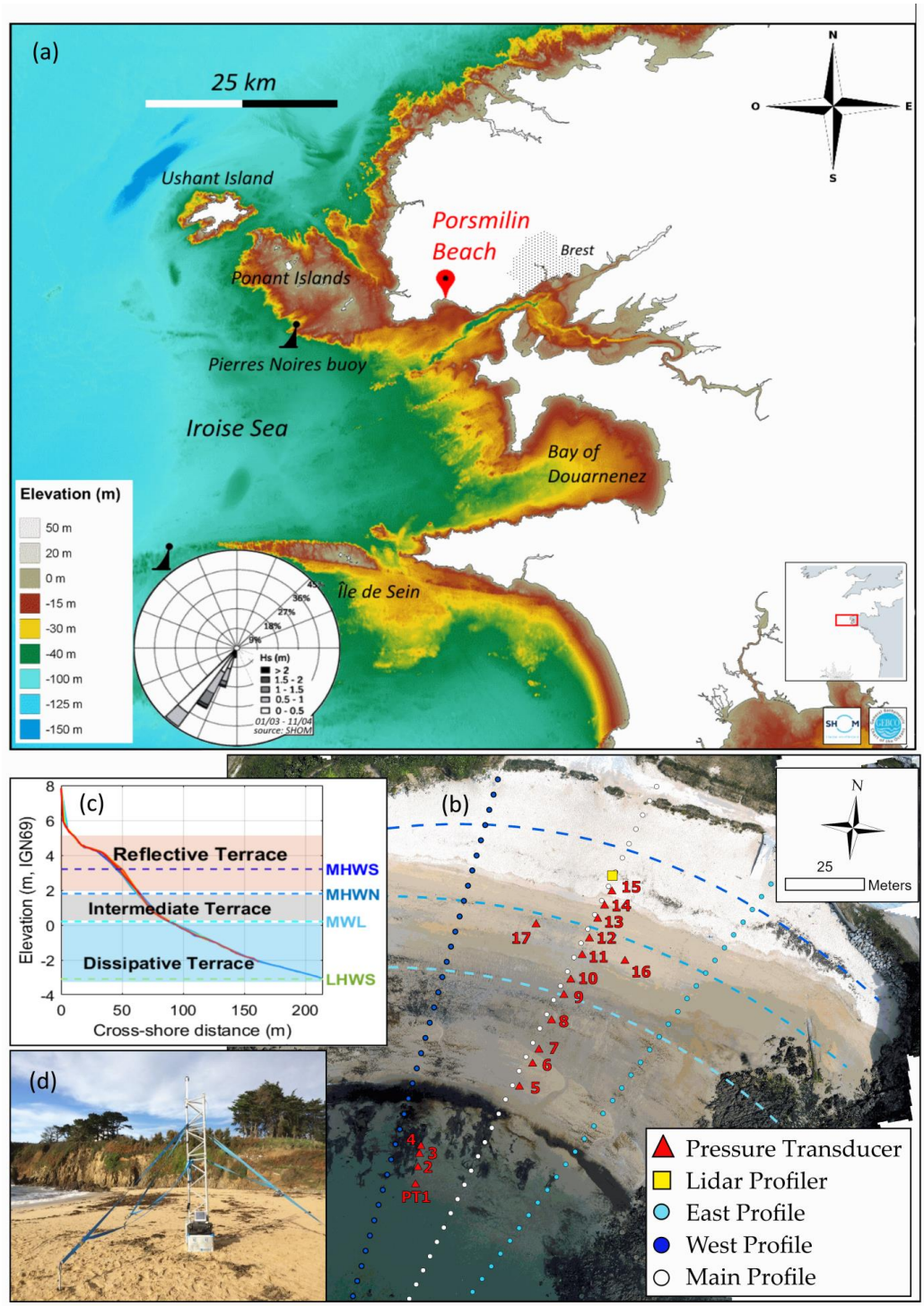

Figure 1. (**a**) Location of Porsmilin Beach on the French Atlantic coast, sheltered in Bertheaume Bay with swell rose of one year's measurements made at the 'Pierres Noires' buoy. Swells are mainly south-west and present low-to-mild energetic conditions (bathymetry data from Homonim project, [27,30]. (**b**) An illustration of the Porsmilin Beach profile with the positions of the pressure transducers (PTs), east and west DGPS profiles, and the main profile. (**c**) The cross-shore profile of Porsmilin Beach based on IGN69, with the elevations of characteristic water levels (MLWS: Mean Low Water Spring; MWL: Mean Water Level; MHWN: Mean High Water Neap; MHWS: Mean High Water Spring). (**d**) Photograph showing the location of the LiDAR installation on the beach profile.

3. Results

3.1. Wave and Tidal Conditions

Our first finding based on wave height observations was the strong tidal modulation of the signal (Figure 2). This occurs because the significant height is modulated by the height of the water. During low tides, dissipation on the seabed is accentuated, resulting in a reduction in Hs. Between 14 and 15 October, the significant wave height (Hs) measured was approximately 1.2 m with a period of 14 s. Subsequently, both the height and period decreased, reaching Hs = 0.4 m and T = 7 s on 17 (and 18) October. During three episodes on 21 October, the average period reached 14 s with a peak Hs of around 1.2 m. Another event occurred around 24 October with an Hs of around 1 m. The average period exceeded 14 s during two other events, with a peak of 14.5 s and Hs = 1.3 m reached on 20 October and a peak of 15 s reached on 30 October. This period lasted only three tides in neap (21, 22, and 23). Between 1 and 2 November, the significant wave height decreased from 0.4 to 0.1 m with a period of less than 10 s. These long swells are a result of the fourteenth and fifteenth tropical cyclones of the 2016 season in the North Atlantic. Specifically, the storms Matthew (28 September–9 October) and Nicole (4–18 October), which originated in the North Atlantic, affected coastal areas of the Iroise Sea. These storms are subsequently used as references to characterize the observed wave forcing during the campaign. The shape of the waves, described here by Sk and As, presents a tidal cyclic signature and varies inversely. *Sk* shows more significant variability, especially during long swell episodes (Figure 2). The asymmetry (Figure 2d) and skewness (Figure 2e) of the waves exhibit similar cyclic variations, with higher values during spring tides. This indicates that the wave shapes are more deformed and asymmetric during these periods. During neap tides, the waves appear more symmetrical and less energetic.

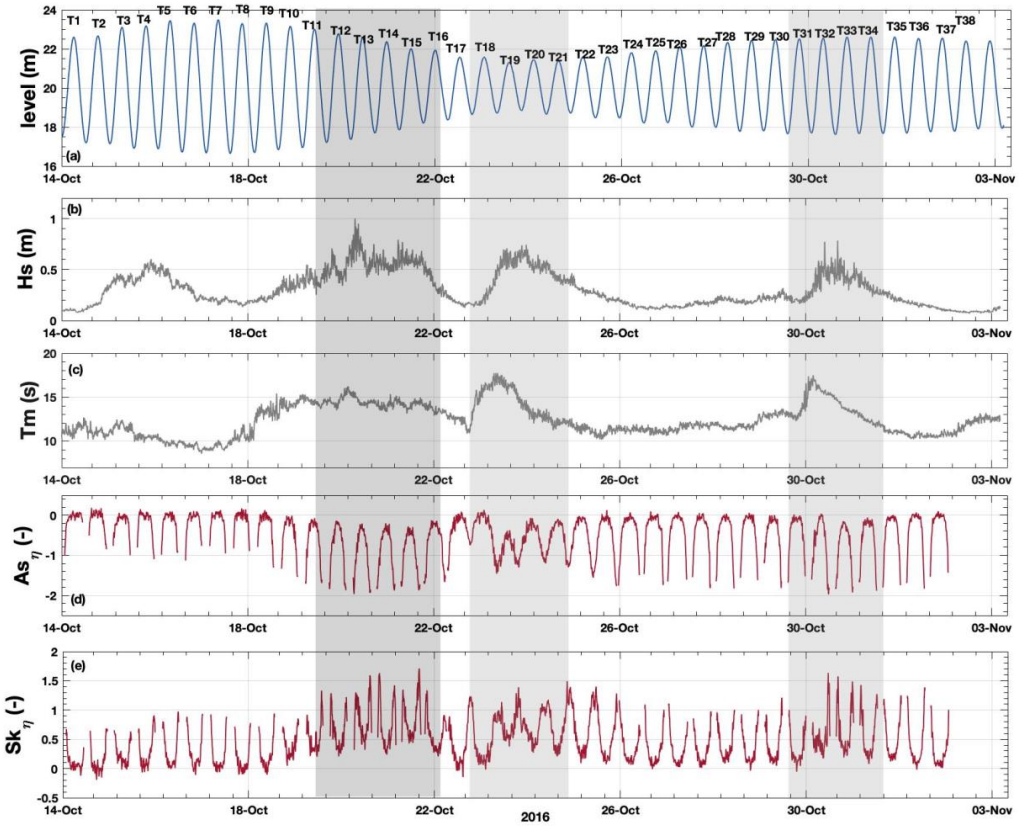

Figure 2. Tidal and swell conditions recorded by the off-shore sensor located 2 km from the beach. (**a**) Variation in the tidal water level. (**b**) Variation in the significant wave height. (**c**) Variation in the mean wave period. (**d**,**e**) Evolution of asymmetry and skewness at PT1. Storm episodes are indicated by the grey zones.

3.2. Wave Shape Variability on the Cross-Shore Profile

This section examines the non-linear characteristics of waves during high tide using the asymmetry (As_η) and skewness (Sk_η) parameters from Equation (3). In the initial phase of the investigation, we focussed our attention on high tides, which facilitate the acquisition of simultaneous data across the entire profile since all the sensors are submerged. It can be observed that the values of As_η and Sk_η remain low and stable as long as the significant wave height (Hs) remains constant (Figure 3). However, in the shoaling zone where Hs increases slightly, the absolute values of As_η and Sk_η rise, indicating steeper waves that are more likely to break as expected [21].

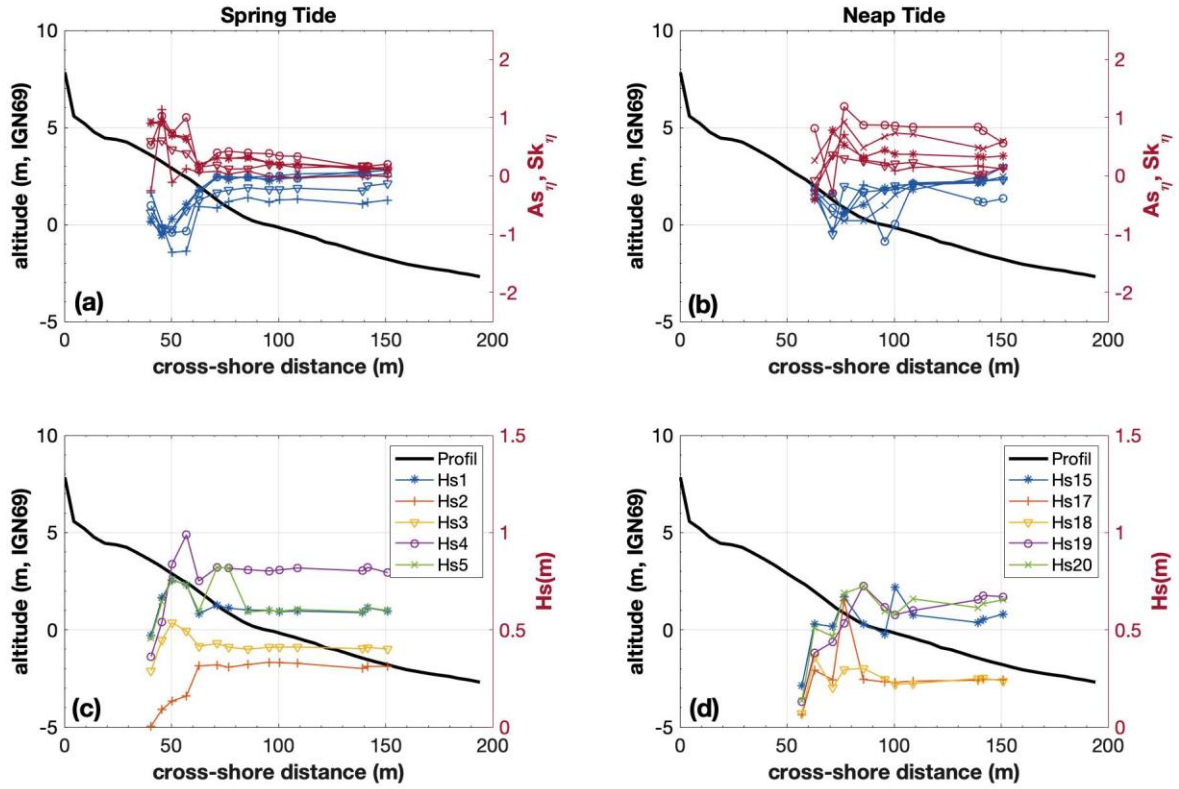

Figure 3. Cross-shore variation in non-linearity parameters (asymmetry (blue) and skewness (red)) and significant wave height at different tides for G1. (**a**) shows the cross-shore variation in As_η and Sk_η for tides T1, T2, T3, T4, and T5. (**b**) shows the cross-shore variation in As_η and Sk_η for tides T15, T17, T18, T19 and T20. (**c**) shows the cross-shore variation in Hs for tides T1, T2, T3, T4, and T5. (**d**) shows the cross-shore variation in Hs for tides T15, T17, T18, T19 and T20.

3.3. Influence of the Breaking Position on Non-Linearity

In order to study the influence of the breaking position on the non-linearities, three groups were defined. Group G1 gathered the period when breaking occurred between PT 9 and PT11, Group 2 (G2) between PT6 and PT7, and Group 3 (G3) between PT4 and PT5. In addition, each group corresponded to different sea states, including spring tides, neap tides, and mean tides. Figure 4 shows the evolution of the asymmetry and skewness for groups G1, G2, and G3 along the cross-shore profile, referenced by the relative water depth (hr), defined as the ratio of the local depth (h) to the depth at the breaking point (hb). Thus, hr = 1 at the breaking location.

The highest non-linearity peaks were observed in the upper part of the beach, between the surf zone and the swash zone. For instance, during the second tide, the maximum values of asymmetry (As_{max} = 0.26) and skewness (Sk_{max} = 1.138) were reached at 41 m with an Hs of 0.28 m. During the T24 tide of G2, the asymmetry reached a significant peak at 77 m (As_{max} = 2.42), surpassing the values of the other wave groups. G3 exhibited

elevated values of asymmetry (As_{max} = 0.6477) at 46.11 m and skewness (Sk_{max} = 1.764) at 50.8 m following the breakpoint during tide 13.

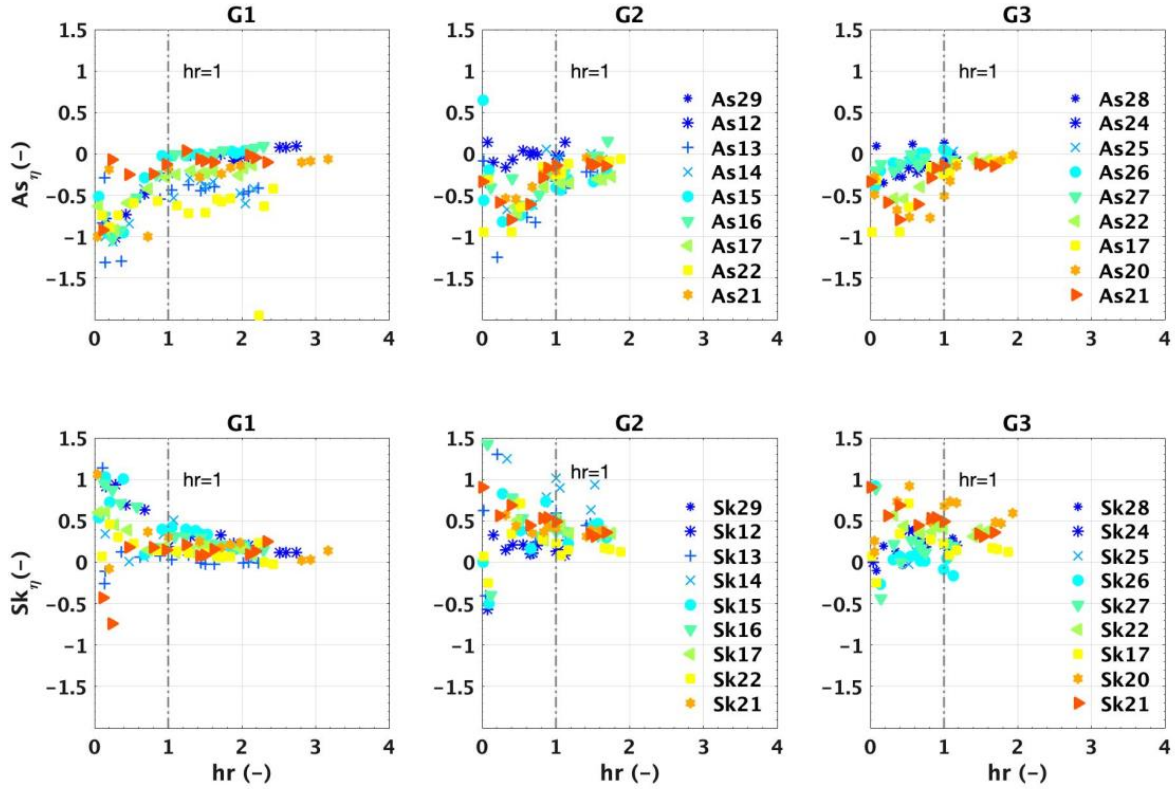

Figure 4. Asymmetry and skewness for groups G1, G2, and G3 along the cross-shore profile referenced by relative water depth (hr) (an hr value of 1 (grey dashed line) indicates the local wave-breaking position).

Non-linearities were more significant during the periods of high hydrodynamic agitation. During moderate periods, we observe an almost linear variation in the skewness and asymmetry in the shoaling zone. This was manifested by a more significant variation in the skewness compared with the asymmetry across the entire intertidal zone. For example, during tides 12 and 13 (between October 20 and 21), the skewness reached peaks of 1.2 and 1.3 at depths of less than 1 metre. In contrast, during spring tides, the skewness varied only slightly at depths between 1 and 6 metres. The skewness then increased slightly between the surf zone and the swash zone. Figure 4 also demonstrates a significant variation in the asymmetry and skewness in the surf zone (for hr < 1).

4. Discussions

The main objective of this study was to investigate the relationship between the evolution of wave non-linearities during their propagation towards the beach and the local slope of Porsmilin Beach. To achieve this, data from 15 pressure transducers were used to evaluate wave non-linearity evolution along a cross-shore macrotidal beach profile by calculating the asymmetry and skewness of the free surface. The beach profile was analyzed using the topographical data obtained through DGPS (Differential Global Positioning System) measurements. The spectral analysis and spatial evolution of significant wave height were used to identify the wave-breaking point (refer to Section 3.2). It is clear that slope and energy play a modulating role in the different types of wave breaking on the beach, with plunging breakers occurring rapidly on the upper beach during high tide, and spilling breakers occurring more slowly towards the lower beach during medium and low tide.

4.1. The Influence of Slope on Non-Linearities

Ref. [21] has demonstrated numerically that the slope influences the maximum value of B reached at a high Ursell number, leading to their updated parametrization (Equation (8)). The maximum value of B is shown numerically to evolve as a polynomial function of NP0 (Equation (9)). This section will examine the maximum values of the measured non-linearity parameters (As_{max}, Sk_{max}, and B_{max}), as well as the non-linearity parameters at the breaking point ($As_{breaking}$ and $Sk_{breaking}$). Figure 5 shows these values against NP0, separated according to their location on the cross-shore profile (dissipative terrace, intermediate part, or reflective part of the beach). The maximum values of As and Sk are observed in the vicinity of the wave-breaking point, particularly between the surf and swash zones on the upper beach where significant wave height (Hs) exhibits considerable variability (refer to Sections 3.2 and 3.3, Figure 3). In this area, there is a rapid increase in wave asymmetry and a concomitant decrease in skewness. The impact of gentler slopes (0.02–0.04) on short-wave non-linearity is less pronounced, whereas steeper sections exhibit greater non-linearity (Figure 5). Furthermore, the degree of asymmetry decreases as the beach slope increases in accordance with the findings of [13]. This indicates that steeper slopes lead to greater wave reflection, which in turn reduces non-linearities and delays breaking.

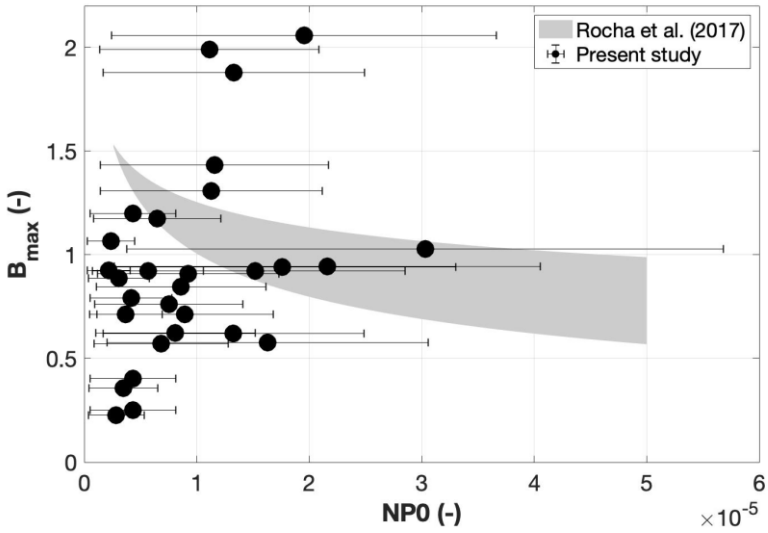

Figure 5. Bmax as a function of NP0 (the bars represent the variability with slope across the beach), the grey shade represents the [8] formula within a 95% confidence interval.

Ref. [8] introduced the combination parameter B to quantify wave non-linearity. This provides a global and dimensionless measure. They also proposed NP0 to model non-linearities based on beach slope and off-shore wave steepness. The present study evaluated NP0 using off-shore sensor data. We found that Sk_{max} and $Sk_{breaking}$ increase with NP0, reaching a plateau for very low NP0 values (NP0 (10^{-5})), which is an order of magnitude lower than the NP0 (10^{-4}) scale of [8]. In contrast, As_{max} and $As_{breaking}$ decrease rapidly with increasing NP0. The correlation between NP0 and Sk_{max} or As_{max} is very poor. The presence of an inhomogeneous slope distribution, particularly an initial break at d = 77 m, may contribute to this. A correlation of 0.58 is observed between $As_{breaking}$ and slope at the top of the beach, 0.57 at the bottom, and 0.55 in the middle, indicating that asymmetry at the breaking point decreases as the beach steepens. This might be due to greater wave reflection reducing non-linearities [13]. Maximum skewness values are more intense for low NP0 values. Figure 5 shows our data as well as [8]'s formula for Bmax (shaded area representing the 95% confidence interval). Our data does not follow the same trend as this numerical study. All these observations reveal that the beach slope may have a more important influence on non-linearities than expected, and not only on the value of Bmax.

4.2. Parameterization

Regarding the influence of the Ursell number on the asymmetry parameter (As), the data obtained from both instruments indicate a reduction in value with an increase in Ur (Figure 6a). The pressure data exhibit greater scatter, but both instruments indicate a convergence towards lower asymmetry values at high Ur (Figure 6). LiDAR represents a single high tide, and it explains the lack of scattering. The scatter in the pressure data (gathering many days so many different off-shore conditions) means that the Ursell number alone is not sufficient to explain non-linearity variability. However, the classical mean wave parameters do not explain this scattering. The authors of [16] show that this scatter is caused by differences in wave-breaking and non-linear energy transfer rate. It investigates as well the influence of the gradients of tidal current but, considering that our investigated zone is flanked by a cliff, the tidal current is negligible and so is its gradient.

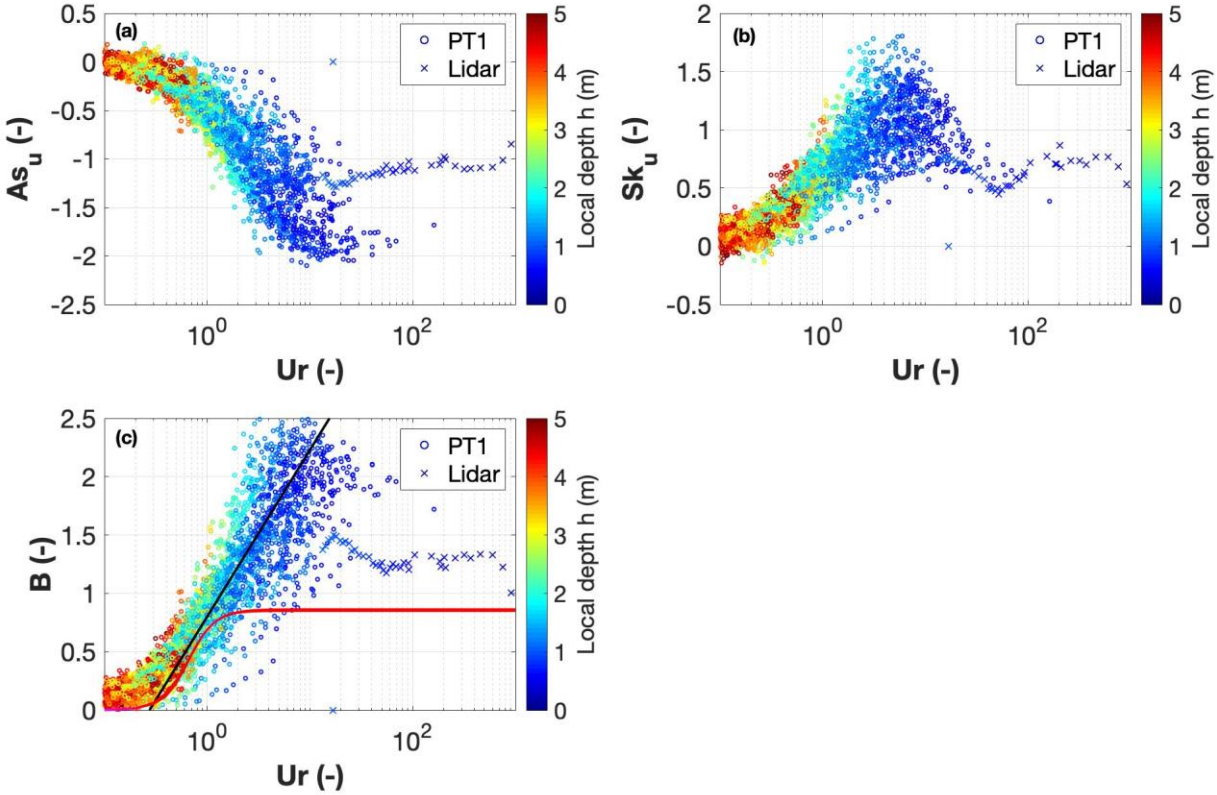

Figure 6. Wave non-linearity parameters As_u on (**a**), Sk_u on (**b**), B, B_{DB95} (black line, Equation (7)), and B_{R12} (red line, Equation (8)) including the slope effect from [26] (**c**). The LiDAR data are represented by crosses (x), while the PT1 data are represented by circles. The color scale indicates the local depth (h) in meters, from blue (0 m) to red (5 m).

Regarding skewness (Sk), it increases up to about one for Ur about five and a decrease is then observed, consistent with LiDAR data. For B, our data closely follow the trend observed by [18] up to Ur = 1. For higher Ursell numbers, our data follow the formula of [19] before converging to a limit value of B for Ur > 20 higher than the value expected with [18]'s formula even including the slope effect from [21] (Figure 6c).

We consider now only B and its variability regarding the location of sensors across the beach (Figure 7). Pressure transducers PT1 and PT5 were positioned on the dissipative part of the beach (slope from 0.01 to 0.03), while PT8 and PT11 were positioned on the reflective part of the beach (slope 0.08). If the data from PT1 are quite aligned with [17]'s formula, the data seem more and more shifted to higher Ursell numbers. This shift has already been observed by [20] who hypothesized a delayed response of the wave to the slope, inducing

that an Ursell number calculated over a deeper location should be used (leading us to consider a lower Ursell number and thus to shift the curve to match [18]'s formula).

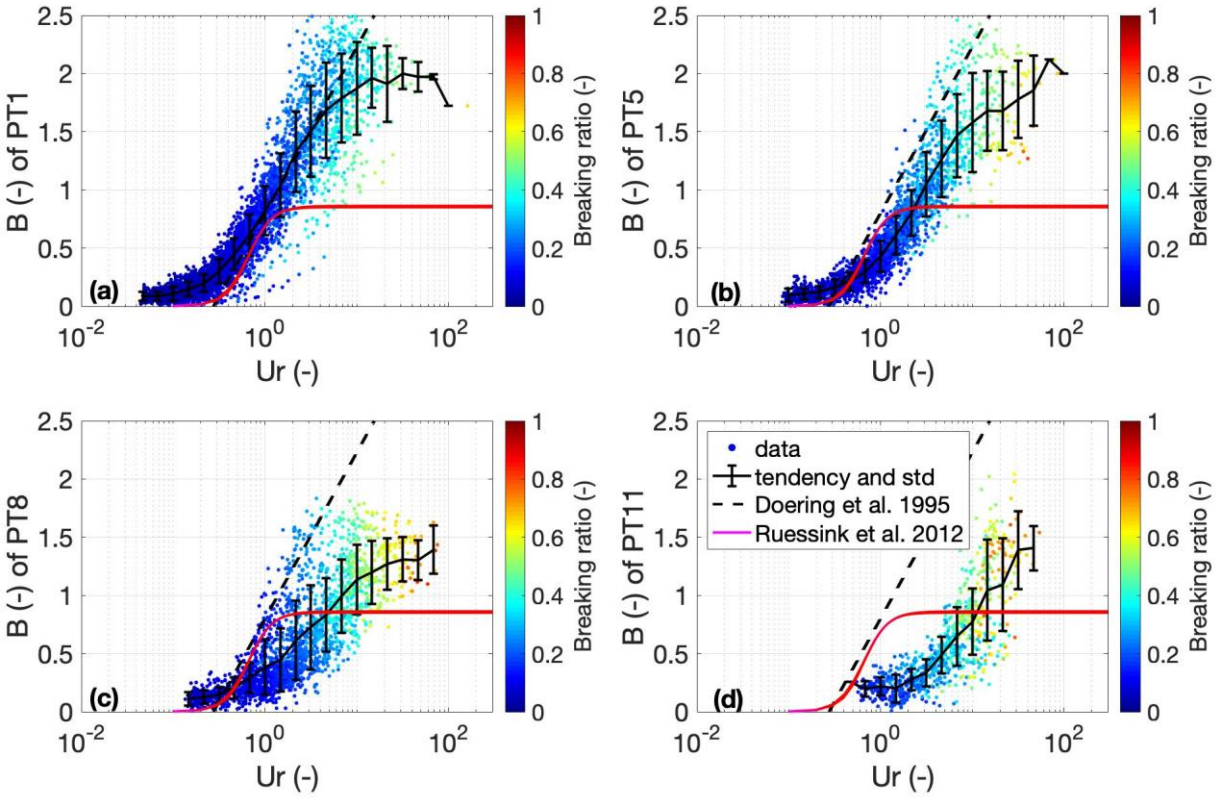

Figure 7. Comparison of the calculated data with other established methods for different pressure transducers (PTs) placed along the cross-shore profile of the beach. The *x*-axis represents the Ursell number (Ur), and the *y*-axis shows the non-linearity parameter (B). The color gradient indicates the breaking ratio. Our data, represented by the points, show the observed values for (**a**) PT1, (**b**) PT5, (**c**) PT8 and (**d**) PT11. The black curve with error bars indicates the trend and standard deviation (std) of our data. The dashed curve represents the method of [17], while the red curve indicates the method of [18].

In Figure 8, the dashed black line represents the parameterization proposed by [17]. The solid red line represents the outcomes yielded by the methodology proposed by [18]. The curves ranging from black to light grey illustrate the non-linearity estimated from the linear wave theory, demonstrating the transition from off-shore (or low tide terrace) to the coast (or reflective part of the beach).

Figure 8 gathers the B calculated for every 15 pressure transducers, highlighting the progressive shift from lower to upper beach. The maximum value of B reached for high Ursell numbers is always higher than the one predicted by the formula from the literature. This value has been shown to be influenced as well by the bed slope [20], but the proposed parameterization is not sufficient to match the value observed.

An increasing deviation between in situ observations and the discussed parameterization is found when moving closer towards the shore. Using an adapted local Ursell number $Ur^* = 3\ H_{m0}{}^*\ k^*/(8(k^*h^*)^3)$ considering deeper water instead of local water depth as performed by [20] brings together all the curves and shows good agreement with the parameterization of [25] for Ur between 0.1 and 1.5. For Ur > 1.5, the data corresponds to a breaking ratio > 0.4 which corresponds to the breaking zone on this beach [20]. Considering $h^* = h + \Delta h$, it is possible to link the ratio $\Delta h/h$ and the bed slope as demonstrated in Figure 9. The current data show some variability around the trend line, but generally adhere to this linear trend. Similarly, the data from [20] align well with this trend, indicating

that both data sets support the same relationship between Δh/h and β. At first order, a linear trend allows us to adapt the parameterization of [18] using an Ur* number for a depth h* = h (1 + β/0.08). This parameterization represents more efficiently the influence of slope than those of [8] that underestimate this influence in our natural environment. The influence of slope on the non-linearities using [20] is quite weak compared with what we observed in situ at this low-tide terrace beach. In future numerical models modeling beach morphodynamics, the spatial and seasonal variability of beach slope should be considered to calculate the wave non-linearity influence on sediment transport.

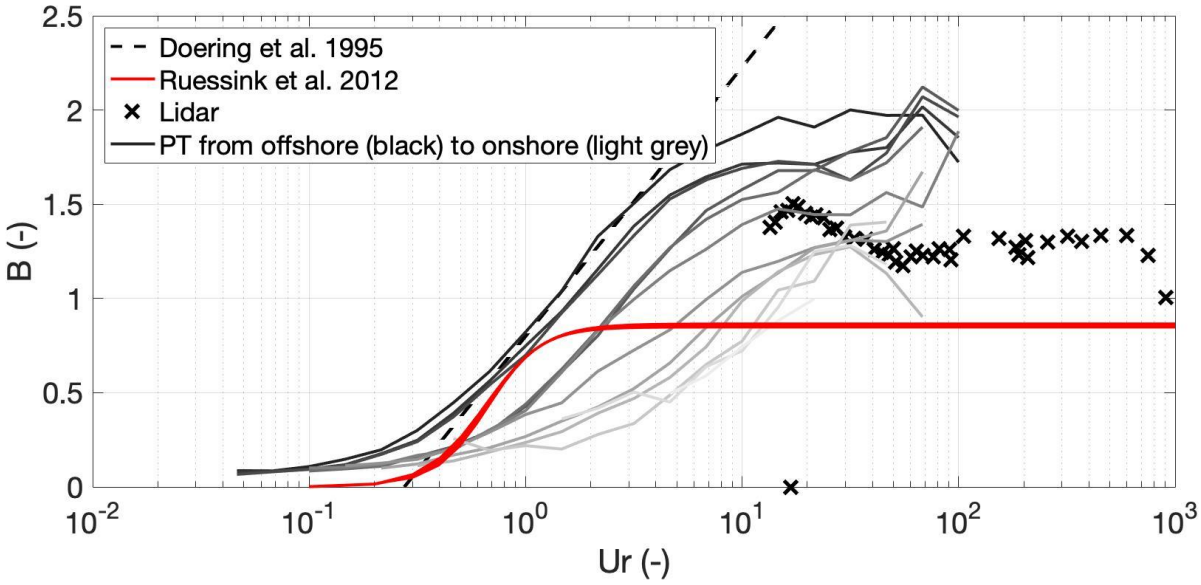

Figure 8. Mean curves for each PT ranging from off-shore (black) to near-shore (light grey). Compared with [17] (dashed line) and [18] (red line), the LiDAR data in the swash zone obtained from one high tide are also shown (crosses).

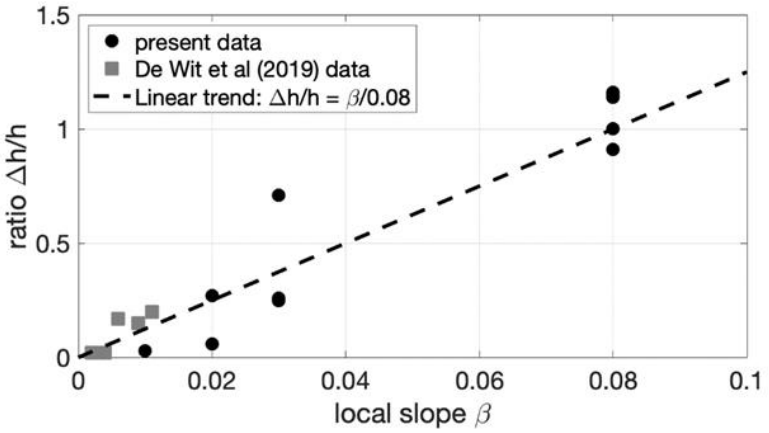

Figure 9. Comparison of current data with data from [20]: relationship between local slope (β) and ratio (Δh/h).

This comparison elucidates the strengths and limitations of each parameterization method for capturing wave non-linearities, thereby emphasizing the necessity of considering site-specific data to enhance the accuracy of wave modeling in coastal environments. Areas with more sloppy bottoms should also be investigated, as should pebble beaches. However, the influence of the substrate porosity may also have an influence on the wave transformation and thus wave shape.

5. Conclusions

The results of this study demonstrate the significance of parameterizing the non-linearities of waves as they propagate along a low-tide terrace beach. Wave shape parameters, such as asymmetry and skewness, vary along the cross-sectional profile of the beach, reaching maximum values around the wave-breaking point. We observed that beach sections with a gentler slope have less impact on wave non-linearity, while steeper sections exhibit greater non-linearity. By comparing the extracted shape parameters with traditional parameterizations, the study demonstrates the efficacy of these parameters in a highly dynamic area, the macrotidal environment, over a topography that fluctuates spatially. Furthermore, the study elucidated the impact of beach slope on the morphology of waves propagating along the cross-shore profile. Considering an Ursell number for a higher water depth, as if the wave answer was delayed, allows us to better capture the evolution of wave non-linearities. We show that this spatial shift is linearly linked to the local beach slope. These observations underline the intricate interplay between beach morphology, wave characteristics, and failure processes. They highlight the necessity of integrating these parameters into coastal dynamics models to better model the sediment transport induced by wave non-linearities.

Author Contributions: Conceptualization, F.F.; methodology, F.F., C.C. and E.A.; software, A.D., E.A. and F.F.; validation, F.F., B.A.S., A.D., E.A. and C.C.; formal analysis, A.D. and F.F.; investigation, A.D.; data curation, A.D. and F.F.; writing—original draft preparation, A.D.; writing—review and editing, A.D., F.F. and C.C.; visualization, A.D.; supervision, F.F., B.A.S. and C.C. All authors have read and agreed to the published version of the manuscript.

Funding: ANR DIME (ANR-10-IEED-0006-14), EUR ISblue (ANR-17-EURE-0015), LabexMER (ANR-10-LABX-19), ANR WEST (ANR-20-CE01-0009).

Data Availability Statement: Data available in a publicly accessible repository. The data presented in this study are openly available at https://doi.org/10.35110/74ecce0a-e650-4c41-9970-97e4602f1cd8 (accessed on 16 October 2024).

Acknowledgments: The authors wish to thank all those who have contributed to the success of this work: coastal dynamics team and instruments from P2I, The Interdisciplinary Graduate School for the Blue Planet (ISblue). We gratefully acknowledge the financial support from ANR DIME (ANR-10-IEED-0006-14), EUR ISblue (ANR-17-EURE-0015), Institut National des Sciences de l'Univers (DYNATREZ project), LabexMER (ANR-10-LABX-19) and ANR WEST (ANR-20-CE01-0009).

Conflicts of Interest: The authors declare no conflicts of interest.

References

1. McGranahan, G.; Balk, D.; Anderson, B. The rising tide: Assessing the risks of climate change and human settlements in low elevation coastal zones. *Environ. Urban.* **2007**, *19*, 17–37. [CrossRef]
2. Athanasiou, P.; Van Dongeren, A.; Giardino, A.; Vousdoukas, M.; Gaytan-Aguilar, S.; Ranasinghe, R. Global distribution of nearshore slopes with implications for coastal retreat. *Earth Syst. Sci. Data* **2019**, *11*, 1515–1529. [CrossRef]
3. Luijendijk, A.; Hagenaars, G.; Ranasinghe, R.; Baart, F.; Donchyts, G.; Aarninkhof, S. The state of the world's beaches. *Sci. Rep.* **2018**, *8*, 6641. [CrossRef] [PubMed]
4. Rey-valette, H.; Carbonnel, P.; Roussel, S.; Faculté, L.; Economiques, S.; De, A.; Site, M. L' apport de la gestion integree des zones cotieres (gizc) a la gestion de l' erosion cotiere: Intérêt et exemple en Méditerranée française. *VertigO-la Rev. Électron. Sci. l'Environ.* **2006**, *7*, 1–12.
5. Wright, L.D.; Short, A.D. Morphodynamic variability of surf zones and beaches: A synthesis. *Mar. Geol.* **1984**, *56*, 93–118. [CrossRef]
6. Masselink, G.; Short, A.D. The effect of tide range on beach morphodynamics and morphology: A conceptual beach model. *J. Coast. Res.* **1993**, *9*, 785–800.
7. van der A, D.A.; O'Donoghue, T.; Ribberink, J.S. Measurements of sheet flow transport in acceleration-skewed oscillatory flow and comparison with practical formulations. *Coast. Eng.* **2010**, *57*, 331–342. [CrossRef]
8. Rocha, M.V.L.; Michallet, H.; Silva, P.A. Improving the parameterization of wave nonlinearities—The importance of wave steepness, spectral bandwidth and beach slope. *Coast. Eng.* **2017**, *121*, 77–89. [CrossRef]
9. Nielsen, P. *Coastal Bottom Boundary Layers and Sediment Transport*; World Scientific: London, UK, 1992.

10. Henderson, S.M.; Allen, J.S. Nearshore sandbar migration predicted by an eddy-diffusive boundary layer model. *J. Geophys. Res. C Ocean.* **2004**, *109*, 1–15. [CrossRef]
11. Berni, C.; Barthélemy, E.; Michallet, H. Surf zone cross-shore boundary layer velocity asymmetry and skewness: An experimental study on a mobile bed. *J. Geophys. Res. Ocean.* **2013**, *118*, 2188–2200. [CrossRef]
12. Fromant, G.; Hurther, D.; van der Zanden, J.; van der A, D.A.; Cáceres, I.; O'Donoghue, T.; Ribberink, J.S. Wave Boundary Layer Hydrodynamics and Sheet Flow Properties Under Large-Scale Plunging-Type Breaking Waves. *J. Geophys. Res. Ocean.* **2019**, *124*, 75–98. [CrossRef]
13. Nielsen, P. Sheet flow sediment transport under waves with acceleration skewness and boundary layer streaming. *Coast. Eng.* **2006**, *53*, 749–758. [CrossRef]
14. Aagaard, T.; Hughes, M.; Baldock, T.; Greenwood, B.; Kroon, A.; Power, H. Sediment transport processes and morphodynamics on a reflective beach under storm and non-storm conditions. *Mar. Geol.* **2012**, *326–328*, 154–165. [CrossRef]
15. Filipot, J. Investigation of the Bottom-Slope Dependence of the Nonlinear Wave Evolution toward Breaking Using SWASH. *J. Coast. Res.* **2015**, *32*, 1504. [CrossRef]
16. van der Lugt, M.A.; de Schipper, M.A.; Reniers, A.J.H.M.; Ruessink, B.G. Parametrizing nonlinearity in orbital velocity at fetch-limited, low-energy beaches. *Coast. Eng.* **2024**, *194*, 104602. [CrossRef]
17. Doering, J.C.; Bowen, A.J. Parametrization of orbital velocity asymmetries of shoaling and breaking waves using bispectral analysis. *Coast. Eng.* **1995**, *26*, 15–33. [CrossRef]
18. Ruessink, B.G.; Ramaekers, G.; Van Rijn, L.C. On the parameterization of the free-stream non-linear wave orbital motion in nearshore morphodynamic models. *Coast. Eng.* **2012**, *65*, 56–63. [CrossRef]
19. Bowen, A.J.; Doering, J.C. Nearshore sediment transport: Estimates from detailed measurements of the nearshore velocity field. In Proceedings of the International Nineteenth Coastal Engineering Conference, Houston, TX, USA, 3–7 September 1984; Edge, B.L., Ed.; ASCE: New York, NY, USA, 1985; Volume II, pp. 1703–1714. [CrossRef]
20. de Wit, F.; Tissier, M.; Reniers, A. Characterizing wave shape evolution on an ebb-tidal shoal. *J. Mar. Sci. Eng.* **2019**, *7*, 367. [CrossRef]
21. Rocha, M.; Silva, P.; Michallet, H.; Abreu, T.; Moura, D.; Fortes, J. Parameterizations of wave nonlinearity from local wave parameters: A comparison with field data. *J. Coast. Res.* **2013**, *65*, 374–379. [CrossRef]
22. Pierson, W.J.; Marks, W. The power spectrum analysis of ocean-wave records. *Eos Trans. Am. Geophys. Union* **1952**, *33*, 834–844.
23. Elgar, S.; Guza, R.T.; Raubenheimer, B.; Herbers, T.H.C.; Gallagher, E.L. Spectral evolution of shoaling and breaking waves on a barred beach. *J. Geophys. Res. Ocean.* **1997**, *102*, 15797–15805. [CrossRef]
24. Longuet-Higgins, M.S.; Cleaver, R.P.; Fox, M.J.H. Crest instabilities of gravity waves: Part 2. Matching and asymptotic analysis. *J. Fluid Mech.* **1994**, *259*, 333–344. [CrossRef]
25. Guza, R.T. Observations of bispectra of shoaling surface gravity waves. *J. Fluid Mech.* **1985**, *161*, 425–448. [CrossRef]
26. Floc'h, F.; Le Dantec, N.; Lemos, C.; Cancouët, R.; Sous, D.; Petitjean, L.; Bouchette, F.; Ardhuin, F.; Suanez, S.; Delacourt, C. Morphological response of a Macrotidal Embayed Beach, Porsmilin, France. *J. Coast. Res.* **2016**, *1*, 373–377. [CrossRef]
27. Caulet, C. Les Plages Sableuses en Environnement Macro-Tidal: De L'Influence de la Pente sur les Processus Morphodynamiques. Ph.D. Thesis, University of Western Brittany, Brest, France, 2018. Available online: https://tel.archives-ouvertes.fr/tel-02139367 (accessed on 7 December 2018).
28. Lemos, C.; Floc'h, F.; Yates, M.; Le Dantec, N.; Marieu, V.; Hamon, K.; Cuq, V.; Suanez, S.; Delacourt, C. Equilibrium modeling of the beach profile on a macrotidal embayed low tide terrace beach. *Ocean. Dyn.* **2018**, *68*, 1207–1220. [CrossRef]
29. Bertin, S.; Floc'h, F.; Le Dantec, N.; Jaud, M.; Cancouët, R.; Franzetti, M.; Cuq, V.; Prunier, C.; Ammann, J.; Augereau, E.; et al. A long-term dataset of topography and nearshore bathymetry at the macrotidal pocket beach of Porsmilin, France. *Sci. Data* **2022**, *9*, 79. [CrossRef]
30. SHOM. MNT Bathymétrique de Façade Atlantique (Projet Homonim). 2015. Available online: https://diffusion.shom.fr/donnees/bathymerie/mnt-facade-atl-homonim.html (accessed on 23 September 2024).